Nanoscale Advances

PAPER

View Article Online
View Journal | View Issue

Cite this: *Nanoscale Adv.*, 2019, **1**, 1186

Influence of interlayer interactions on the relaxation dynamics of excitons in ultrathin MoS_2

Dongxiao Lu, [ab] Qiang Zhou,*[a] Fangfei Li,[a] Xiaowei Li [c] and Geyu Lu*[b]

Received 12th July 2018
Accepted 17th December 2018

DOI: 10.1039/c8na00086g

rsc.li/nanoscale-advances

Interlayer interactions play a crucial role in modifying the optical and electronic properties of layered materials in a complex way, which is of key importance for the performance of the optoelectronic devices based on these novel materials. In this contribution, we performed an investigation into the underlying influence of interlayer interactions on the relaxation dynamics of excitons in ultrathin MoS_2 using the femtosecond transient absorption spectroscopy technique. The experimental results manifest that interlayer interactions in bilayer MoS_2 can largely facilitate the exciton–phonon scattering process and inhibit the radiative recombination process, which consequently accelerates the relaxation rate of A excitons and results in the decrease of the relaxation lifetime of A excitons in bilayer MoS_2.

1. Introduction

Two-dimensional layered transition-metal dichalcogenides (TMDs) have attracted growing attention in recent decades due to their remarkable optical and electronic properties. Unlike the zero band gap of graphene, TMDs have potential advantages in optoelectronic devices in virtue of their intrinsic semiconductor characteristics with a sizable band gap. As a typical TMD semiconductor with a bandgap of 1.2–2 eV, molybdenum disulphide (MoS_2) exhibits fascinating optical properties, such as strong exciton luminescence,[1,2] large exciton binding energy,[3,4] and valley polarization.[5,6] As such, MoS_2 has been widely applied in light emitting diodes,[7–9] photodiodes,[10–12] solar cells,[13–15] and field effect transistors.[16–18] It is generally known that each molecular layer of MoS_2 is constructed with a molybdenum-atom layer sandwiched between two sulfur-atom layers by strong covalent bonds. Such strong covalent bonding endows MoS_2 with excellent mechanical strength and a high thermal stability up to 1090 °C in an inert environment.[19] Additionally, adjacent layers of MoS_2 are coupled to each other by weak van der Waals interactions, which enables MoS_2 to be created layer by layer and to exhibit diverse novel physical properties.

It is well acknowledged that the photoelectric properties and exciton properties of two-dimensional layered MoS_2 depend sensitively on the number of layers, and the interlayer interaction plays a crucial role in determining the unique electronic,[20] optical[21] and exciton[22] properties of layered materials in a complex way. Therefore, in this regard, understanding the underlying influence of interlayer interactions on the optical and electrical properties of two-dimensional layered MoS_2 is particularly important. However, most of the interlayer interaction-relevant theoretical and experimental studies, such as the investigation regarding the effect of interlayer interactions on the molecular structure,[23,24] on the band gap,[25] and on optical properties[26] are performed on multilayer MoS_2 or bulk MoS_2, which may introduce some unnecessary interference. Moreover, in spite of some recent investigations on the effects of interlayer interactions on steady-state optical properties of ultrathin MoS_2,[27] the influences of interlayer interactions on transient optical properties, especially on the ultrafast relaxation dynamics of excitons are still unknown, which however are of key importance for realizing potential applications of the novel ultrathin MoS_2.

In this contribution, to shed light on the underlying influences of interlayer interactions on the relaxation dynamics of excitons in ultrathin MoS_2, we conducted a systematic study by analyzing the discrepancy in relaxation dynamics and photoluminescence only between bilayer MoS_2 and monolayer MoS_2. The experimental results indicate that the relaxation dynamics and photoluminescence properties of excitons in bilayer MoS_2 were significantly different from those in monolayer MoS_2 because of the presence of interlayer interactions. For example, in comparison to the monolayer MoS_2, a dramatic reduction of photoluminescence quantum efficiency and a remarkably accelerated relaxation rate of A excitons were observed in bilayer MoS_2. The possible reasons for this special difference were discussed in terms of the effects of interlayer interactions in detail.

[a]State Key Laboratory of Superhard Materials, College of Physics, Jilin University, Changchun 130012, China. E-mail: zhouqiang@jlu.edu.cn

[b]State Key Laboratory of Integrated Optoelectronics, College of Electronic Science and Engineering, Jilin University, 2699 Qianjin Street, Changchun 130012, China. E-mail: lugy@jlu.edu.cn

[c]Center for Advanced Optoelectronic Functional Materials Research, Key Laboratory of UV-Emitting Materials and Technology, Northeast Normal University, Ministry of Education, 5268 Renmin Street, Changchun 130024, China

2. Experimental

2.1. Preparation of two-dimensional layered MoS_2 samples

Monolayer and bilayer MoS_2 samples were synthesized on the surface of a quartz substrate by a chemical vapor deposition (CVD) method using a tube furnace with two separate hot zones.[28] In a typical procedure, two ceramic boats loaded with 700 mg of sulfur powder and 10 mg of MoO_3 powder were first placed at the central part of each tube furnace, as shown in Fig. 1(a and b). To provide a favourable growth atmosphere, the quartz tube was vacuumed and then ultra-pure argon gas was flowed into the reaction tube under a low pressure of about 0.4 atm. Then, the MoO_3 powder was quickly heated to 850 °C at a heating rate of 25 °C min^{-1} and the sulfur powder mildly sublimated at a heating rate of 6 °C min^{-1} to 200 °C. After the two separate hot zones reached to 850 °C and 200 °C, it was going to need another 15 min for MoS_2 growth before finally naturally cooling down to room temperature.

2.2. Characterization

Raman and photoluminescence spectra were detected using a micro-Raman spectrometer (Horiba-JY T64000) with a 100× objective in a back-scattering configuration, using a solid state green laser with 532 nm wavelength as the excitation source. The steady-state absorption spectra were measured using an Ocean Optics QE65000 spectrometer. The layer-dependent signals of relaxation dynamics of excitons were characterized using a self-designed femtosecond transient absorption spectroscopy (fs-TAS) system, as shown in Fig. 2. Our fs-TAS system is composed of a coaxial pump-probe system, white-light probe system and optical imaging system. In brief, a regenerative amplified Ti/sapphire laser (Spectra-Physics) was employed to produce an 800 nm laser pulse characterized by a 35 fs pulse width and a 1 kHz repetition rate. Then the initial output laser beam was split into two beams: the frequency of one beam was doubled to generate the pump beam (400 nm), and the other beam was focused on a 5 mm water container to produce white light acting as a probe pulse. Finally, the probe pulse met with the pump beam and remained coaxial with the pump beam. The radii of the focal spots of the pump and probe beams on the sample were measured to be 9 μm and 5 μm based on the real time observation using an optical microscope. The time delay between the pump and probe beams was achieved with a computer-controlled translation stage (M-405.DG, PI Corp.), and the signal was sent to a lock-in amplifier (SR830, Stanford Co.) to be further processed.

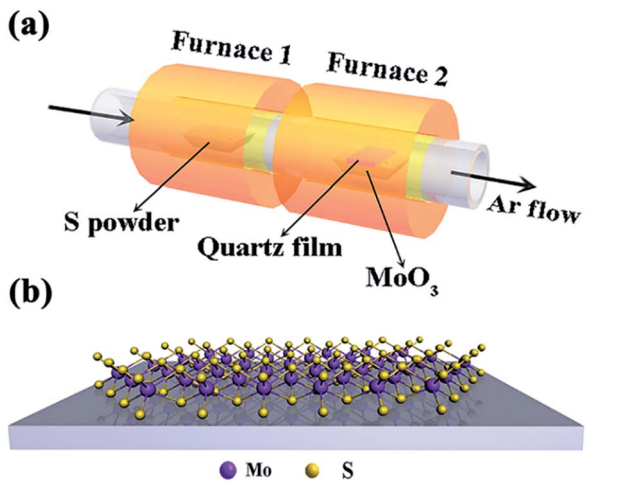

Fig. 1 (a) Schematic illustration of the tube-furnace setup employed in this study for the synthesis of monolayer and bilayer MoS_2; (b) a schematic view of the two-dimensional structures of monolayer MoS_2 on the substrate.

3. Results and discussion

Fig. 3(a) shows the optical micrograph of the as-synthesized MoS_2 samples and it can be seen that the boundaries of different areas are very clear, and the two large homogeneous regions marked '1' and '2' were preliminarily identified to be layered MoS_2. And the sizes of the samples at '1' and '2' are estimated to be about 130 μm^2 and 450 μm^2 with the assistance of a ruler scale. Moreover, to figure out the accurate layer number of the as-obtained MoS_2 samples, Raman spectroscopy was further performed.[29] Fig. 3(b) shows the Raman spectra of the as-synthesized MoS_2 samples located at the regions marked by '1' and '2' in Fig. 3(a). As can be seen, there are five Raman modes detected in the center of the Brillouin zone at region '1', namely, shear mode (E^2_{2g}) at 22.7 cm^{-1}, breathing mode (B^2_{2g}) at 40.27 cm^{-1}, in-plane vibration mode (E^1_{2g}) at 383.54 cm^{-1}, out-of-plane vibration mode (A_{1g}) at 405.46 cm^{-1},[30] and the second-order longitudinal acoustic phonon mode (2LA(M)) at 452.21 cm^{-1}.[31] The positions of the peaks corresponding to these five Raman modes are in good agreement with the Raman eigen-frequency of bilayer MoS_2 reported in a previous report;[32] thus region "1" was identified to be bilayer MoS_2.

Fig. 3(c) shows the schematic diagram of typical bilayer MoS_2 and its corresponding characteristic vibration modes. It is clear that the B^2_{2g} mode corresponds to a rigid-layer movement parallel to the *c* axis, and the E^2_{2g} mode corresponds to a rigid-layer movement perpendicular to the *c* axis. Both of them exist only in two or more layers, so there should be no E^2_{2g} and B^2_{2g} modes when there is only a single layer of MoS_2. Based on the above analysis, it can be seen from Fig. 3(b) that there are only three Raman modes (A_{1g}, E^1_{2g} and 2LA(M)) detected in the Raman spectra for region '2', and the absence of E^2_{2g} and B^2_{2g} Raman signals implied that the region '2' is monolayer MoS_2.[33]

Fig. 4(a) presents the UV-vis absorption spectra of the monolayer and bilayer MoS_2. As can be seen, there are two prominent absorption bands centered at 660 and 618 nm for both monolayer and bilayer MoS_2. By contrast, the intensity of the absorption bands of bilayer MoS_2 is much stronger than that of monolayer MoS_2. The absorption band centered at 660 nm is well indexed to A excitons' absorption, while the absorption band around 618 nm can be indexed to B excitons' absorption.[34] The absorption of A and B excitons is generally believed to be derived from the optical transition from the valence bands (K_{v1} and K_{v2}) to the minimum of the conduction band (K_c) at the *K* point in the Brillouin zone, respectively, as

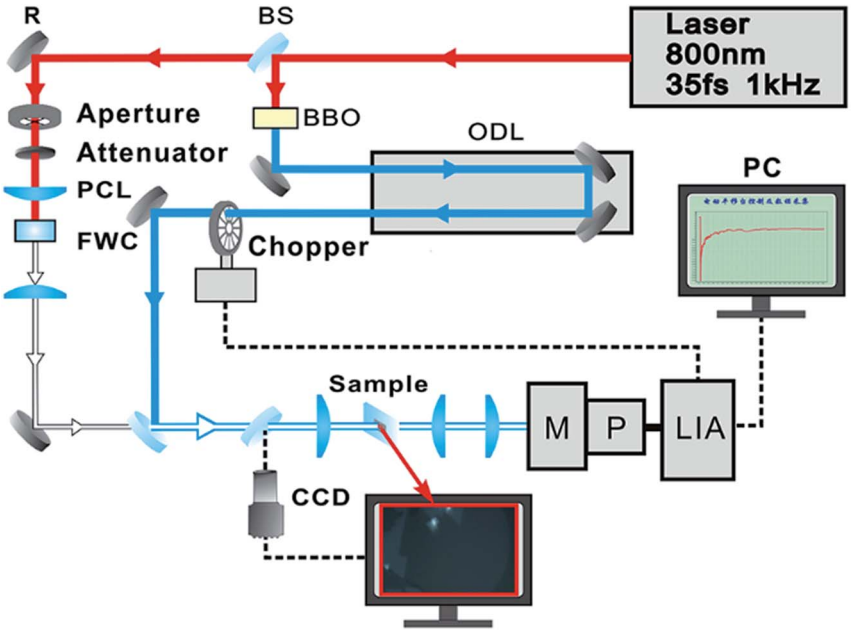

Fig. 2 The schematic diagram of a femtosecond transient absorption spectroscopy system: BS_1 and BS_2, 3 : 7 and 1 : 1 beam splitter; BBO, 0.5 mm-thick β-BaB_2O_4 crystal; ODL, optical delay line; R, reflector; CL, convex lens; FWC, flow water cell; M, three grating monochromator; P, photomultiplier; LIA, lock-in amplifier.

schematically shown in Fig. 4(b). In addition, the energy difference between K_{v1} and K_{v2} bands stems from the splitting of the maximum valence band,[35,36] which is believed to be caused by the combined effects of interlayer interactions and spin–orbit coupling for bilayer MoS_2 and only the effect of spin–orbit coupling for monolayer MoS_2.[22,37]

In spite of the above well-discussed different stable-state absorption properties of excitons caused by interlayer interactions, the influence of interlayer interactions on the relaxation dynamics of excitons in MoS_2 still remains unknown and needs to be further addressed. Thus the influence of the interlayer interaction on exciton relaxation dynamics was further investigated with the assistance of our self-designed femtosecond transient absorption spectroscopy (fs-TAS) platform. Since the resonance absorption of A excitons for both monolayer and bilayer MoS_2 was around 660 nm as shown in

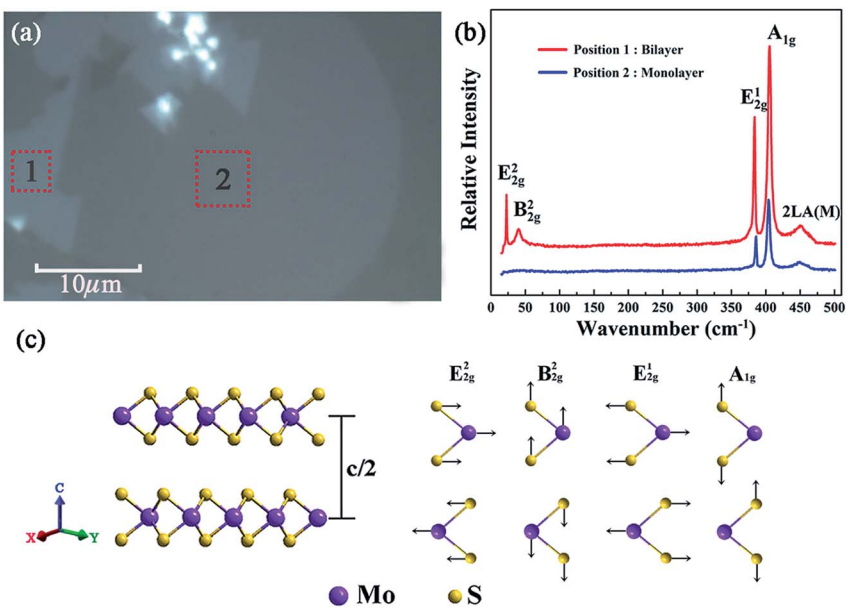

Fig. 3 (a) Optical micrograph of layered MoS_2 samples deposited on the quartz substrate; (b) Raman spectra of the as-synthesized MoS_2 samples in the regions marked '1' and '2' in (a); (c) schematic diagrams of the lattice structure (left side) in out-of-plane directions of MoS_2 and its corresponding characteristic Raman vibration modes (right side).

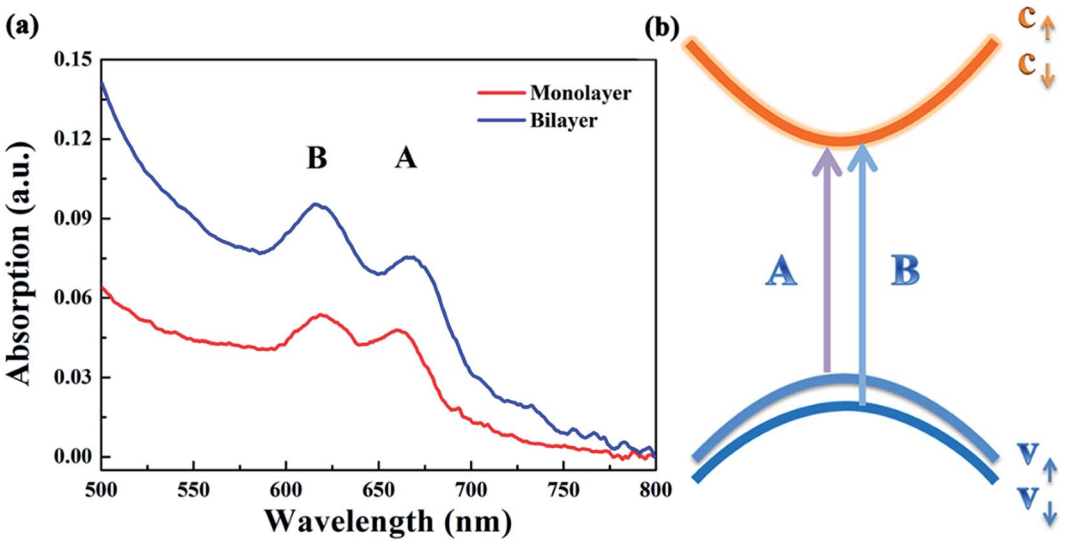

Fig. 4 (a) The UV-vis absorption spectra of the as-grown monolayer and bilayer MoS_2 after being returned to zero at 800 nm; (b) simplified band structure of MoS_2 at the *K* point in the Brillouin zone.

the UV-vis absorption spectra in Fig. 4(a), the probe laser wavelength was chosen to be 660 nm during the fs-TAS measurements. Besides, to guarantee the formation of photo-excited excitons at the A exciton level, the pump laser wavelength was set at 400 nm. And the pump intensity was selected to be 2 μJ cm^{-2} according to the linear relationship between the signal intensity and pump intensity (Fig. 5) to get strong and steady signals.

Fig. 6(a) displays the relaxation dynamics curves of A excitons for monolayer and bilayer MoS_2. It is noteworthy that the relaxation time of bilayer MoS_2 was much shorter than that of monolayer MoS_2, which implies that the whole exciton relaxation became faster in the presence of interlayer interactions. Furthermore, the decay curves of monolayer and bilayer MoS_2 were fitted separately and the fitting parameters for the decay curves are summarized in Table 1. As can be seen, both the relaxation dynamics signals of monolayer and bilayer MoS_2 exhibit multi-exponential decays and can be fitted very well using a three exponential Gaussian response function of $a_1 \cdot \exp(-t/\tau_1) + a_2 \exp(-t/\tau_2) + a_3 \exp(-t/\tau_3)$, where $\tau_1 < \tau_2 < \tau_3$, which implies that multiple relaxation processes were involved. For monolayer MoS_2, the decay was characterized by a fast decay time constant (τ_1) of 3.3 ± 0.1 ps, an intermediate decay time constant (τ_2) of 82.9 ± 5.6 ps and a slow decay time constant (τ_3) of 1053.9 ± 26.6 ps, the proportion of the above three time constants was 35%, 20% and 45% in turn. Moreover, the relaxation lifetime of monolayer MoS_2 is 489.5 ± 13.1 ps, which is close to the values in the literature,[38] while for bilayer MoS_2, the decay time constant was composed of a fast decay (τ_1) of 3.7 ± 0.1 ps (31% weight), an intermediate decay (τ_2) of 42.4 ± 0.8 ps (51% weight), and a slow decay (τ_3) of 714.4 ± 25.1 ps (18% weight), and the relaxation lifetime is 150.7 ± 4.9 ps. The obviously changed proportion of the decay time constant and the significantly reduced relaxation lifetime for bilayer MoS_2 imply that interlayer interactions have a significant effect on the relaxation characteristics of excitons.

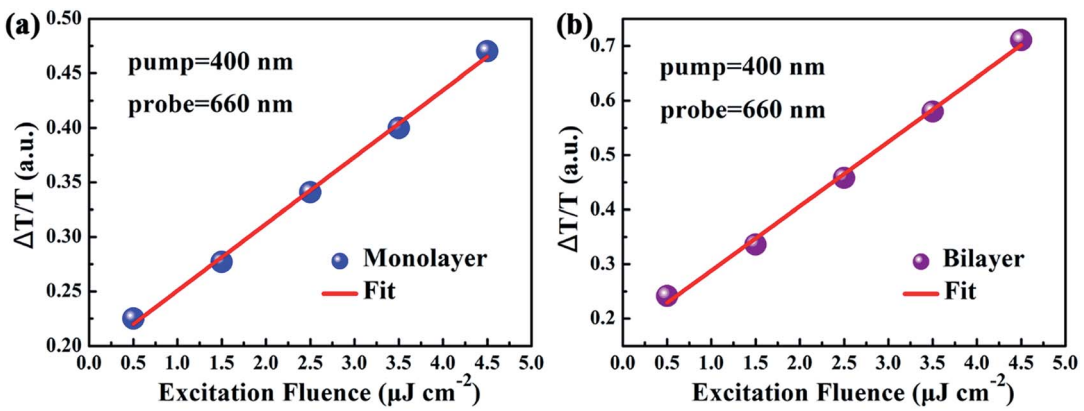

Fig. 5 Signal intensity of $\Delta T/T$ at zero time delay as a function of excitation intensity for (a) monolayer and (b) bilayer MoS_2 with a pump wavelength of 400 nm and a probe wavelength of 660 nm. The circles denote the experimental data, while the solid lines denote the linear fitting data.

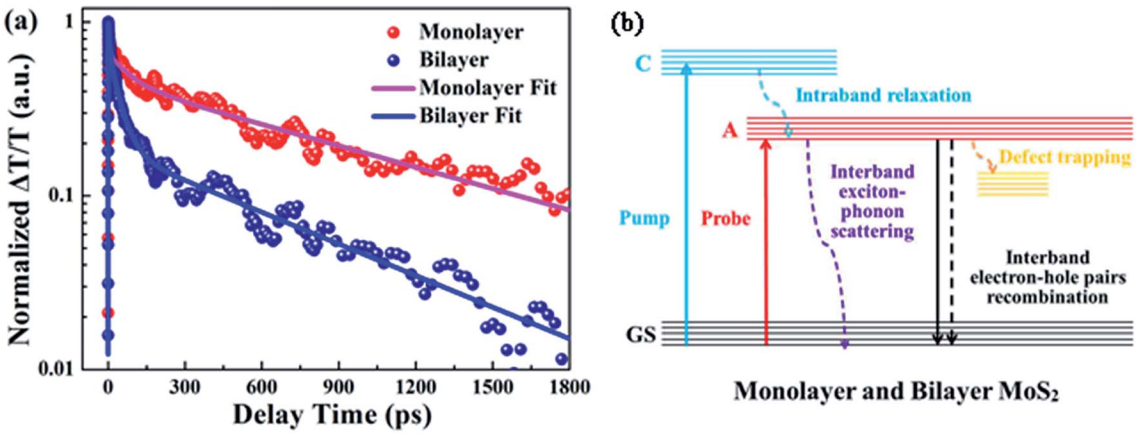

Fig. 6 (a) Experimental (solid circles) and fitted (thick lines) data for normalized transient absorption relaxation dynamics curves of monolayer and bilayer MoS_2. All the relaxation dynamics curves were normalized at time zero, being fitted with a three exponential function $I(t) = a_1 \exp(-t/\tau_1) + a_2 \exp(-t/\tau_2) + a_3 \exp(-t/\tau_3)$; (b) schematic summary of relaxation processes in monolayer and bilayer MoS_2.

Table 1 Fitting parameters for decay curves in Fig. 6(a) using a Gaussian response function with the three-exponential decay functions of $I(t) = a_1 \exp(-t/\tau_1) + a_2 \exp(-t/\tau_2) + a_3 \exp(-t/\tau_3)$ with the fitting uncertainty. The percentage in the brackets represents the proportion of τ_1, τ_2 and τ_3

	τ_1 (ps)	τ_2 (ps)	τ_3 (ps)	Lifetime (ps)
Monolayer	3.3 ± 0.1 (35%)	82.9 ± 5.6 (20%)	1053.9 ± 26.6 (45%)	489.5 ± 13.1
Bilayer	3.7 ± 0.1 (31%)	42.4 ± 0.8 (51%)	717.4 ± 25.1 (18%)	150.7 ± 4.9

To shed light on the underlying mechanism for the above dramatic reduction of the exciton relaxation time observed in bilayer MoS_2, the transient absorption decay dynamics of monolayer and bilayer MoS_2 were further characterized at different pump intensities, and the normalized dynamics curves are shown in Fig. 7. It can be seen that no significant dynamics dependences on the pump intensity were observed in either monolayer or bilayer MoS_2, which indicates that the fast decay component was not the exciton–exciton annihilation process in this work. Since shallow and deep traps usually exist in MoS_2 nanoclusters,[39] and the fast decay time (τ_1) obtained here is similar to the time scale of defect trapping;[40] thus the fast decay component observed here was closely related to fast defect trapping. In addition, considering the characteristics of ultrathin MoS_2, the exciton–phonon interaction is going to be very significant in monolayer and bilayer MoS_2. Since the intermediate decay time constant (τ_2) in our work was of the same order as the exciton–phonon scattering time reported in a recent study,[40] the intermediate decay observed here might be attributed to the exciton–phonon scattering. The slowest decay process that lasted for hundreds of picoseconds (τ_3) is generally believed to be derived from the recombination of electrons and holes. The schematic of the relaxation processes involved in monolayer and bilayer MoS_2 is shown in Fig. 6(b).

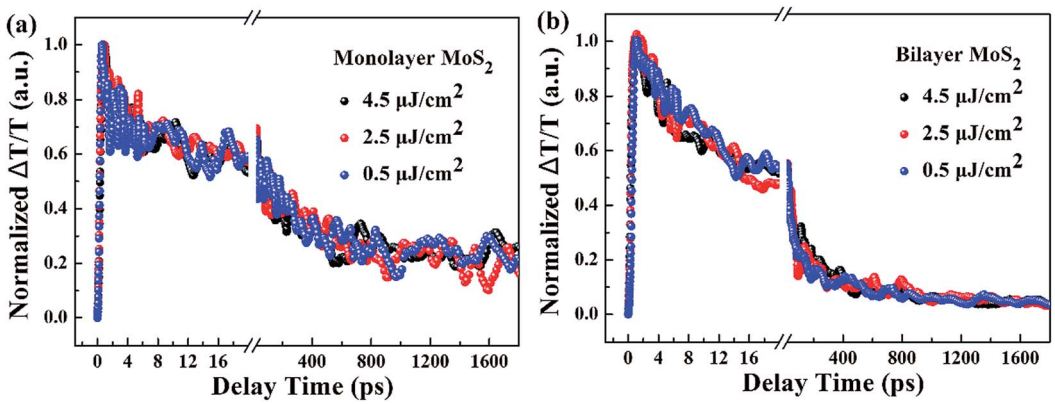

Fig. 7 Normalized transient absorption decay dynamics curves of (a) monolayer and (b) bilayer MoS_2 with a pump wavelength of 400 nm and a probe wavelength of 660 nm at different pump intensities.

It is worth noting that unlike the similar values of τ_1, the values of τ_2 and τ_3 for bilayer MoS_2 were both significantly lower than those for monolayer MoS_2. This dramatic enhancement of the exciton relaxation rate observed in bilayer MoS_2 might be understood by the following aspects. Firstly, as can be seen from Fig. 3(b), the additional Raman vibration modes (B^2_{2g} and E^2_{2g}) and the stronger Raman vibration mode of A_{1g} in bilayer MoS_2 imply that the vibration of the atoms and lattice was enhanced due to the presence of interlayer interactions in comparison to monolayer MoS_2.[41] And the enhanced vibration of the lattice caused by the interlayer interaction will facilitate the exciton–phonon scattering in bilayer MoS_2, resulting in a shorter intermediate decay time τ_2.

Secondly, since monolayer MoS_2 is a direct band-gap semiconductor, most of the electrons and holes are located on the conduction band minimum (CBM) and valence band maximum (VBM) at the *K* point, respectively; thus the radiative recombination of electrons and holes happens very easily, which can be verified by the extremely strong photoluminescence (PL) intensity of monolayer MoS_2 as shown in Fig. 8. Therefore, the main recombination process of electrons and holes in monolayer MoS_2 is radiative recombination. However, bilayer MoS_2 is an indirect band-gap semiconductor, the photon energy (3.1 eV) employed here will pump the initial carriers to a higher energy level, and the fast cooling of the carriers would let the electrons and holes locate on the CBM at the *K* point and the VBM at the *Γ* point,[2] respectively. Thus, the radiative recombination of electrons and holes in bilayer MoS_2 requires the assistance of phonons,[42] which will significantly suppress the radiative relaxation process in bilayer MoS_2. Moreover, many previous reports have proved that the interlayer interaction can redistribute the charges , which gives rise to a local electric field at the interfacial region in bilayer MoS_2. After being excited by the pump beam, the electrons will accumulate at the interfacial surfaces, while the holes will thus be pushed away from the interface due to the local electric field, which will lead to spatial separation of electrons and holes. And the reduction of the overlap between electron and hole wavefunctions will make the relaxation of electrons and holes through radiative recombination difficult, resulting in the decrease of fluorescence quantum yield.[27] This can also be seen in the PL spectra shown in Fig. 8. It can be seen from Fig. 8 that the PL intensity of A excitons reduced dramatically in bilayer MoS_2, which suggests that the radiative recombination becomes negligible in bilayer MoS_2 compared to monolayer MoS_2. Therefore, the prominent recombination process of electrons and holes in bilayer MoS_2 is non-radiative recombination. Furthermore, it is well known that the decay time of non-radiative recombination is usually shorter than that of radiative recombination.[43,44] Therefore the decay time τ_3 of bilayer MoS_2 is much shorter than that of monolayer MoS_2. Given the above, it therefore can be concluded that the dramatic enhancement of the whole relaxation rate of A excitons for bilayer MoS_2 can be explained by the combined effects of the enhanced exciton–phonon scattering and reduced radiative relaxation induced by interlayer interactions.

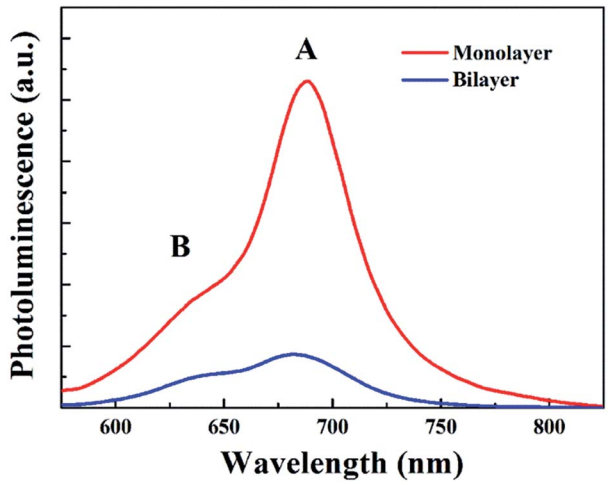

Fig. 8 Photoluminescence (PL) spectra of monolayer and bilayer MoS_2.

4. Conclusions

In summary, we performed a detailed investigation into the underlying influence of interlayer interactions on the relaxation dynamics of excitons in ultrathin MoS_2 by analyzing the discrepancy in relaxation dynamics and photoluminescence properties only between bilayer MoS_2 and monolayer MoS_2. On the basis of thoughtful analysis about the obtained experimental data, both monolayer and bilayer MoS_2 samples exhibit multiple relaxation processes involving the defect trapping, the exciton–phonon scattering, and the recombination process of electrons and holes. Moreover, the characterization results manifest that the relaxation rate of A excitons was significantly accelerated in bilayer MoS_2 compared to monolayer MoS_2, which is due to the combined effects of the enhanced exciton–phonon scattering and reduced radiative relaxation induced by interlayer interactions.

Conflicts of interest

There are no conflicts to declare.

Acknowledgements

We are grateful to Prof. Yisong Zheng and Prof. Jianzhong Zhang for many fruitful discussions. We also thank Prof. Kai Wang and researcher Guohui Lu for their help during the experimental research. This work was supported by the financial support from the National Natural Science Foundation of China (no. 11274137, 11574112, 11474127, 51304080).

References

1 K. F. Mak, C. Lee, J. Hone, J. Shan and T. F. Heinz, *Phys. Rev. Lett.*, 2010, **105**, 136805.
2 X. M. Dou, K. Ding, D. S. Jiang and B. Q. Sun, *ACS Nano*, 2014, **8**, 7458–7464.

3 A. R. Klots, A. K. M. Newaz, B. Wang, D. Prasai, H. Krzyzanowska, J. H. Lin, D. Caudel, N. J. Ghimire, J. Yan, B. L. Ivanov, K. A. Velizhanin, A. Burger, D. G. Mandrus, N. H. Tolk, S. T. Pantelides and K. I. Bolotin, *Sci. Rep.*, 2014, **4**, 6608.
4 N. Saigal, V. Sugunakar and S. Ghosh, *Appl. Phys. Lett.*, 2016, **108**, 132105.
5 T. Cao, G. Wang, W. P. Han, H. Q. Ye, C. R. Zhu, J. R. Shi, Q. Niu, P. H. Tan, E. Wang, B. L. Liu and J. Feng, *Nat. Commun.*, 2012, **3**, 887.
6 K. F. Mak, K. L. He, J. Shan and T. F. Heinz, *Nat. Nanotechnol.*, 2012, **7**, 494–498.
7 G. L. Frey, K. J. Reynolds, R. H. Friend, H. Cohen and Y. Feldman, *J. Am. Chem. Soc.*, 2003, **125**, 5998–6007.
8 G. J. Choi, Q. V. Le, K. S. Choi, K. C. Kwon, H. W. Jang, J. S. Gwag and S. Y. Kim, *Adv. Mater.*, 2017, **29**, 1702598.
9 K. P. Guo, C. F. Si, C. Han, S. H. Pan, G. Chen, Y. Q. Zheng, W. Q. Zhu, J. H. Zhang, C. Sun and B. Wei, *Nanoscale*, 2017, **9**, 14602–14611.
10 Y. X. Deng, Z. Luo, N. J. Conrad, H. Liu, Y. J. Gong, S. Najmaei, P. M. Ajayan, J. Lou, X. F. Xu and P. D. Ye, *ACS Nano*, 2014, **8**, 8292–8299.
11 Y. Niu, R. Frisenda, S. A. Svatek, G. Orfila, F. Gallego, P. Gant, N. Agrait, C. Leon, A. Rivera-Calzada, D. P. De Lara, J. Santamaria and A. Castellanos-Gomez, *2D Mater.*, 2017, **4**, 034002.
12 Z. Li, J. H. Chen, R. Dhall and S. B. Cronin, *2D Mater.*, 2017, **4**, 015004.
13 X. Gu, W. Cui, H. Li, Z. W. Wu, Z. Y. Zeng, S. T. Lee, H. Zhang and B. Q. Sun, *Adv. Energy Mater.*, 2013, **3**, 1262–1268.
14 M. L. Tsai, S. H. Su, J. K. Chang, D. S. Tsai, C. H. Chen, C. I. Wu, L. J. Li, L. J. Chen and J. H. He, *ACS Nano*, 2014, **8**, 8317–8322.
15 A. Capasso, F. Matteocci, L. Najafi, M. Prato, J. Buha, L. Cina, V. Pellegrini, A. Di Carlo and F. Bonaccorso, *Adv. Energy Mater.*, 2016, **6**, 1600920.
16 G. H. Lee, Y. J. Yu, X. Cui, N. Petrone, C. H. Lee, M. S. Choi, D. Y. Lee, C. Lee, W. J. Yoo, K. Watanabe, T. Taniguchi, C. Nuckolls, P. Kim and J. Hone, *ACS Nano*, 2013, **7**, 7931–7936.
17 B. Radisavljevic, A. Radenovic, J. Brivio, V. Giacometti and A. Kis, *Nat. Nanotechnol.*, 2011, **6**, 147–150.
18 H. Ji, H. Yi, J. Seok, H. Kim, Y. H. Lee and S. C. Lim, *Nanoscale*, 2018, **10**, 10856–10862.
19 S. Bertolazzi, J. Brivio and A. Kis, *ACS Nano*, 2011, **5**, 9703–9709.
20 W. S. Yun, S. W. Han, S. C. Hong, I. G. Kim and J. D. Lee, *Phys. Rev. B*, 2012, **85**, 033305.
21 A. Splendiani, L. Sun, Y. B. Zhang, T. S. Li, J. Kim, C. Y. Chim, G. Galli and F. Wang, *Nano Lett.*, 2010, **10**, 1271–1275.
22 T. Cheiwchanchamnangij and W. R. L. Lambrecht, *Phys. Rev. B*, 2012, **85**, 205302.
23 Y. L. Yan, F. F. Li, Y. B. Gong, M. G. Yao, X. L. Huang, X. P. Fu, B. Han, Q. Zhou and T. Cui, *J. Phys. Chem. C*, 2016, **120**, 24992–24998.
24 X. M. Dou, K. Ding, D. S. Jiang, X. F. Fan and B. Q. Sun, *ACS Nano*, 2016, **10**, 1619–1624.
25 S. W. Han, H. Kwon, S. K. Kim, S. Ryu, W. S. Yun, D. H. Kim, J. H. Hwang, J. S. Kang, J. Baik, H. J. Shin and S. C. Hong, *Phys. Rev. B*, 2011, **84**, 045409.
26 A. F. Rigos, H. M. Hill, Y. L. Li, A. Chernikov and T. F. Heinz, *Nano Lett.*, 2015, **15**, 5033–5038.
27 J. G. Kim, W. S. Yun, S. Jo, J. Lee and C. H. Cho, *Sci. Rep.*, 2016, **6**, 29813.
28 Y. H. Lee, X. Q. Zhang, W. J. Zhang, M. T. Chang, C. T. Lin, K. D. Chang, Y. C. Yu, J. T. W. Wang, C. S. Chang, L. J. Li and T. W. Lin, *Adv. Mater.*, 2012, **24**, 2320–2325.
29 T. Sekine, K. Uchinokura, T. Nakashizu, E. Matsuura and R. Yoshizaki, *J. Phys. Soc. Jpn.*, 1984, **53**, 811–818.
30 T. Wieting and J. Verble, *Phys. Rev. B*, 1971, **3**, 4286–4292.
31 H. Li, Q. Zhang, C. C. R. Yap, B. K. Tay, T. H. T. Edwin, A. Olivier and D. Baillargeat, *Adv. Funct. Mater.*, 2012, **22**, 1385–1390.
32 Y. Zhao, X. Luo, H. Li, J. Zhang, P. T. Araujo, C. K. Gan, J. Wu, H. Zhang, S. Y. Quek and M. S. Dresselhaus, *Nano Lett.*, 2013, **13**, 1007–1015.
33 H. Zeng, B. Zhu, K. Liu, J. Fan, X. Cui and Q. Zhang, *Phys. Rev. B*, 2012, **86**, 241301.
34 R. Coehoorn, C. Haas and R. De Groot, *Phys. Rev. B*, 1987, **35**, 6203–6206.
35 B. Evans and P. Young, *Proc. Phys. Soc.*, 1967, **91**, 475–482.
36 J. Wilson and A. Yoffe, *Adv. Phys.*, 1969, **18**, 193–335.
37 R. F. Frindt, *Phys. Rev.*, 1965, **140**, A536–A539.
38 L. Yang, D. Zhong, J. Y. Zhang, Z. P. Yan, S. F. Ge, P. W. Du, J. Jiang, D. Sun, X. J. Wu, Z. Y. Fan, S. A. Dayeh and B. Xiang, *ACS Nano*, 2014, **8**, 6979–6985.
39 R. Doolen, R. Laitinen, F. Parsapour and D. F. Kelley, *J. Phys. Chem. B*, 1998, **102**, 3906–3911.
40 T. Korn, S. Heydrich, M. Hirmer, J. Schmutzler and C. Schuller, *Appl. Phys. Lett.*, 2011, **99**, 102109.
41 C. Lee, H. Yan, L. E. Brus, T. F. Heinz, J. Hone and S. Ryu, *ACS Nano*, 2010, **4**, 2695–2700.
42 H. Dery and Y. Song, *Phys. Rev. B*, 2015, **92**, 125431.
43 L. Y. Pan, Y. L. Zhang, H. Y. Wang, H. Liu, J. S. Luo, H. Xia, L. Zhao, Q. D. Chen, S. P. Xu, B. R. Gao, L. M. Fu and H. B. Sun, *Nanoscale*, 2011, **3**, 2882–2888.
44 M. Palummo, M. Bernardi and J. C. Grossman, *Nano Lett.*, 2015, **15**, 2794–2800.